RSC Advances

PAPER

View Article Online
View Journal | View Issue

Cite this: *RSC Adv.*, 2020, **10**, 11365

Synthesis, crystal structures and magnetic properties of two heterometallic {Ln_8Cr_4} (Ln = Gd^{3+} and Tb^{3+}) complexes with one-dimensional wave chain structure†

Ye-Min Han, Ning-Fang Li, Yan-Zhao Yu, Jia-Peng Cao, Mu-Xiu Yang, Ya-Lin Hong, Run-Kun Kang, Peng Yuan and Yan Xu *

Received 17th February 2020
Accepted 11th March 2020

DOI: 10.1039/d0ra01524e

rsc.li/rsc-advances

Two isomorphic heterometallic 3d–4f cluster-based materials, formulated $[Gd_8Cr_4(IN)_{18}(\mu_3\text{-}O)_2(\mu_3\text{-}OH)_6(\mu_4\text{-}O)_4(H_2O)_{10}]\cdot 13H_2O$ (**1**) and $[Tb_8Cr_4(IN)_{18}(\mu_3\text{-}O)_2(\mu_3\text{-}OH)_6(\mu_4\text{-}O)_4(H_2O)_{10}]\cdot 13H_2O$ (**2**) (abbreviation: {Ln_8Cr_4}: Ln = Gd^{3+} (**1**); Tb^{3+} (**2**); HIN = isonicotinic acid), were achieved by hydro-/solvothermal method through using the ligand HIN. X-ray diffraction analysis illustrates eight lanthanide ions (Ln = Gd^{3+}, Tb^{3+}) and four transition-metal ions (Cr^{3+}) of {Ln_8Cr_4} were constructed from two classical "drum-like" {Ln_4Cr_2} structures associated by organic ligands HIN, displaying a one-dimensional wave chain structure, which is rare. The magnetic properties of {Gd_8Cr_4} were inspected and showed the existence of antiferromagnetic coupling interactions between contiguous metal ions. On top of this, the magnetic entropy change of ΔS_m can attain 23.40 J kg^{-1} K^{-1} (44.90 mJ cm^{-3} K^{-1}) at about 3 K and ΔH = 7 T. Besides, fluorescence measurements of {Tb_8Cr_4} display typical characteristic Tb-based luminescence.

Introduction

The study of heterometallic 3d–4f metal clusters has evoked extensive attention from researchers owing to their structural aesthetic and prominent application in optics and magnetism.[1–10] Focused on 3d or 4f compounds, 3d–4f clusters combine the properties of different metal atoms in the same molecule, which can lead to tailorable topologies and interesting magnetic properties.[11–13] As far as we know, magnetic refrigeration occurs because of the phenomenon named the magnetocaloric effect (MCE), which relies on the variation of isothermal magnetic entropy ($-\Delta S_m$) as well as adiabatic temperature ($-\Delta T_{ad}$) under different applied magnetic field (ΔH).[14–16] Magnetic materials as one of the most prevalent materials in the field of materials science, have always been a hotspot for their potential applications in environmentally friendly magnetic refrigeration materials with marvelous MCE.[5,15,16] In order to acquire large $-\Delta S_m$, it is natural that a magnetic cooler should possess a high spin ground state, a large magnetic density and negligible magnetic anisotropy.[17] Based on the above considerations, 3d–Gd metal clusters can be a good candidate to trigger a large MCE.[18,19]

By introducing 3d metal ions into lanthanide clusters can not only exhibit a more superior nature, but also have a broad application prospect in fields, including light, electricity, magnetism and catalysis.[9,10] At present, more and more 3d–Gd metal clusters with large MCE have been prepared, ranging from molecular clusters to multi-dimensional coordination polymers where the maximum $-\Delta S_m$ attains 42.8 J kg^{-1} K^{-1} at 3 K for ΔH = 7 T.[20–26] Among plentiful 3d ions, Cr^{3+} ions, closing to isotropic, makes them a good selection as a raw material for magnetic refrigerants.[27] But by reason of the inert nature of Cr^{3+} ions, making it has been untoward to combine them with lanthanide ions to synthesis polynuclear complexes and possess captivating structures.[6] Therefore, works on Cr–Ln compounds are seldom been investigated and an effective synthesis to form Cr–Ln compounds has not been developed.

The progress in designing and constructing Cr–Ln compounds with giant MCE has been substantial but also uneven, such as {Cr_4Ln},[27] {Cr_6Ln_2},[28] {Cr_2Ln_3},[29] {Cr_3Ln_3},[30] {Cr_2Ln_4},[17,31] {Cr_4Ln_4},[6,30] {$Cr_{12}Ln_4$},[28] {Cr_2Ln_5},[32] {Cr_4Ln_8}[32] and {Cr_8Ln_8}[15] clusters, where the maximum $-\Delta S_m$ attains 38.33 J kg^{-1} K^{-1} at 2 K for ΔH = 7 T (see detailed in Table 2). Among reported literatures, Cr–Ln compounds have charming structures, it is more common that ring-like {Cr_4Ln_4},[30] {Cr_3Ln_3},[30] cage-like {Cr_6Ln_2},[28] {$Cr_{12}Ln_4$}[28] and wheel-like {Cr_4Ln_8},[32] {Cr_8Ln_8}[15] clusters. Although the charming structures, there are only a few cases of Cr–Ln clusters with more than ten cores up to now.

College of Chemical Engineering, State Key Laboratory of Materials-Oriented Chemical Engineering, Nanjing Tech University, Nanjing 210009, P. R. China. E-mail: yanxu@njtech.edu.cn

† Electronic supplementary information (ESI) available: CCDC 1978142 and 1978143 for compounds 1–2. CCDC 1978142 and 1978143. For ESI and crystallographic data in CIF or other electronic format see DOI: 10.1039/d0ra01524e

Table 1 Crystal data and structure refinements for 1–2

Compound	1	2
Formula	$C_{108}H_{124}Cr_4Gd_8N_{18}O_{71}$	$C_{108}H_{124}Cr_4Tb_8N_{18}O_{71}$
Formula weight	4276.24	4289.60
T (K)	296(2)	296(2)
Crystal system	Triclinic	Triclinic
Space group	$P\bar{1}$	$P\bar{1}$
a (Å)	13.96(2)	13.71(8)
b (Å)	14.47(2)	14.20(8)
c (Å)	21.07(3)	20.60(12)
β (deg)	80.221(16)	80.096(10)
V (Å^3)	4185(10)	3945.4(4)
Z	1	1
D_c (mg m^{-3})	1.697	1.805
μ (mm^{-1})	3.458	3.891
F (000)	2074	2082
θ range (deg)	0.982–25.099	0.989–25.099
Limiting indices	$-16 \leqq h \leqq 16$, $-17 \leqq k \leqq 17$, $-21 \leqq l \leqq 24$	$-16 \leqq h \leqq 16$, $-16 \leqq k \leqq 16$, $-24 \leqq l \leqq 23$
Reflections collected	28 873	28 601
Independent reflections	14 457 [R(int) = 0.0320]	13 881 [R(int) = 0.0336]
Data/restraints/parameters	14 457/95/955	13 881/116/956
GOF	1.061	1.100
R_1[a], wR_2[b] [$I > 2\sigma(I)$]	$R_1 = 0.0346$ w$R_2 = 0.0931$	$R_1 = 0.0310$ w$R_2 = 0.0871$
R_1, wR_2 (all data)	$R_1 = 0.0436$ w$R_2 = 0.1007$	$R_1 = 0.0353$ w$R_2 = 0.0899$

[a] $R_1 = \Sigma||F_o| - |F_c||/\Sigma|F_o|$. [b] w$R_2 = \Sigma[w(F_o^2 - F_c^2)^2]/\Sigma[w(F_o^2)^2]]^{1/2}$.

Based on our group previous study in Cr–Gd compounds, we have done further investigation in the synthesis and magnetism of Cr–Ln compounds. Luckily, two isostructural one-dimensional chain-like compounds, **{Ln$_8$Cr$_4$}** (Ln = Gd^{3+} (**1**); Tb^{3+} (**2**)), were successfully synthesized by hydro-/solvothermal method, which are rare. The birth of these two twelve cores compounds enrich the family of Cr–Ln, which make a contribution to the field in magnetic refrigeration. In this work, magnetic and optical studies were performed on compounds **1** and **2**, respectively. The magnetic study results demonstrate that compound **1** exhibits magnetocaloric effect values at about 3 K under $\Delta H = 7$ T is 23.40 J kg^{-1} K^{-1}. Simultaneously, fluorescence measurements of compound **2** reveal typical characteristic Tb-centered emissions in the visible region.

Experimental section

Materials and physical property studies

All reactants were reagent grade and used as received. The FT-IR spectrum was recorded in the span of 4000–400 cm^{-1} with a Nicolet Impact 410 FTIR spectrometer using pressed KBr pellets. The data of Powder X-ray diffraction (PXRD) ($2\theta = 5$–$50°$) was obtained by a Bruker D8X diffractometer, which configured with monochromatized Cu-K$_\alpha$ (λ = 0.15418 nm) radiation. Thermogravimetric (TG) measurements were performed on a Diamond thermogravimetric analyzer in a flowing N_2 with a heating ratio of 10 °C min^{-1} in the range of 25–1000 °C. The data of magnetic susceptibility was conducted by a Quantum Design MPMS-XL 7 SQUID magnetometer and diamagnetic corrections were estimated by means of Pascal's constants.

X-ray crystallography

The data of compounds **1–2** of the single-crystal X-ray diffraction were collected on a Bruker SMART Apex II CCD diffractometer by means of Mo-Kα radiation (λ = 0.71073 Å) through using ω–2θ scan technique. And then crystalline structures of the two compounds were figured out with the SHELX-2019/3 program package using direct methods and refined by the fullmatrix least-squares minimization.

Synthesis of compounds

[Gd$_8$Cr$_4$(IN)$_{18}$(μ_3-O)$_2$(μ_3-OH)$_6$(μ_4-O)$_4$(H$_2$O)$_{10}$]·13H$_2$O (1). A mixture of Gd_2O_3 (0.1994 g, 0.55 mmol), isonicotinic acid (0.2396 g, 2.00 mmol), $CrCl_3 \cdot 6H_2O$ (0.1464 g, 0.55 mmol) and HCOOH (0.0183 g, 0.35 mmol) was dissolved in distilled water (12 ml). Stirring for 12 h at the ambient temperature and then 2 mol l^{-1} NaOH was added into the above mixture (pH = 4.00). A

Table 2 Comparison of $-\Delta S_m$ for reported Gd-based polymetallic clusters

Complexes	$-\Delta S_m$ (J kg^{-1} K^{-1})	ΔH (T)	T (K)	Ref.
{Cr$_2$Gd$_4$}	38.33	7.0	2.0	31*c*
{Cr$_2$Gd$_3$}	38.3	7.0	2.0	29
{Cr$_2$Gd$_4$}	36.86	7.0	2.0	17
{Cr$_4$Gd$_8$}	33.8	7.0	2.0	32
{Cr$_2$Gd$_5$}	25.2	7.0	5.0	32
{Cr$_4$Gd$_8$}	23.40	7.0	3.0	This work
{Cr$_4$Gd}	18.31	8.0	3.5	27
{Cr$_4$Gd$_4$}	18.08	7.0	3.0	6

Teflon-lined vessel was sealed and raised the vessel to the temperature of 180 °C for 7 days. Cooling the vessel to ambient temperature and then the expected magenta block crystals of **1** were obtained (yield: 31% basis on Gd). Elemental analysis found (%): C 31.19, H 2.69, N 6.06 (calcd (%): C 30.14, H 2.54, N 6.01).

$[Tb_8Cr_4(IN)_{18}(\mu_3\text{-}O)_2(\mu_3\text{-}OH)_6(\mu_4\text{-}O)_4(H_2O)_{10}]\cdot 13H_2O$ (2). The synthesis of compound **1** and **2** was similar to that of **2** except that Gd_2O_3 was used instead of Tb_4O_7 (0.4112 g, 0.55 mmol). (yield: 42% basis on Tb). Elemental analysis found (%): C 30.89, H 2.81, N 6.00 (calcd (%): C 29.53, H 2.67, N 5.94).

Results and discussion

Syntheses

Hydro-/solvothermal synthesis have recently been confirmed as a valid and simple approach to the synthesis of heterometallic 3d–4f metal clusters. Many variables factors have an impact on the final products, for example, the ligand/metal ratio, solvents, pH values, temperature, reaction time and duration. To achieve Cr–Ln compounds, we select Ln_2O_3, $CrCl_3\cdot 6H_2O$, isonicotinic acid, HCOOH, and H_2O as the reactants. In this work, only two isostructural compounds, **{Ln_8Cr_4}** (Ln = Gd^{3+} (**1**); Tb^{3+} (**2**)), were successfully synthesized under hydrothermal conditions. Although HCOOH does not appear in the structure of the final product, but without adding HCOOH in the process of synthesis, we could not get the target product. At the same time, we have also changed other lanthanide sources, such as Er, Ho, Dy and Tb. Unfortunately, no other isomorphic compounds were obtained except for the isomorphic Tb compounds. In addition to this, we tried to replace $CrCl_3\cdot 6H_2O$ with other chromium compounds, but also failed. It is tricky to synthesize the aforesaid compounds, and it perhaps that we do not find appropriate conditions for other isomorphic compounds. The synthesis is carried out at pH value (4.0–4.5) conditions. Moreover, we made attempts to convert the reaction temperature between 80 and 180 °C, but except the given synthesis temperature, no crystals were found (Table 1).

Structure of $[Gd_8Cr_4(IN)_{18}(\mu_3\text{-}O)_2(\mu_3\text{-}OH)_6(\mu_4\text{-}O)_4(H_2O)_{10}]\cdot 13H_2O$ (1)

Compounds **1–2** belong to the triclinic system, *P*1 space group and the two compounds are isomorphic, herein, the structure of compound **1** was taken as the example. In order to describe the structure clearly, free water molecules and H atoms are omitted. As shown on Fig. 1a, **{Gd_8Cr_4}** is composed of four Cr^{3+} cations, eight Gd^{3+} cations, eighteen IN^- anions, two $\mu_3\text{-}O^{2-}$ group, six $\mu_3\text{-}OH^-$ group, four $\mu_4\text{-}O^{2-}$ group, ten coordination water molecules and seven lattice water molecules.

The structural unit **{Gd_8Cr_4}** can be viewed as the interrelation of two **{Gd_4Cr_2}** building units, which are both made of two Cr^{3+} cations and four Gd^{3+} cations, named first building unit and secondary building unit (abbreviation: **FBU** (Fig. 1b) and **SBU** (Fig. 1c). Although two **{Gd_4Cr_2}** building units with the same "drum-like" metallic framework (Fig. 1d and e), there are obvious discrepancy in the coordination modes of HIN ligands. In the

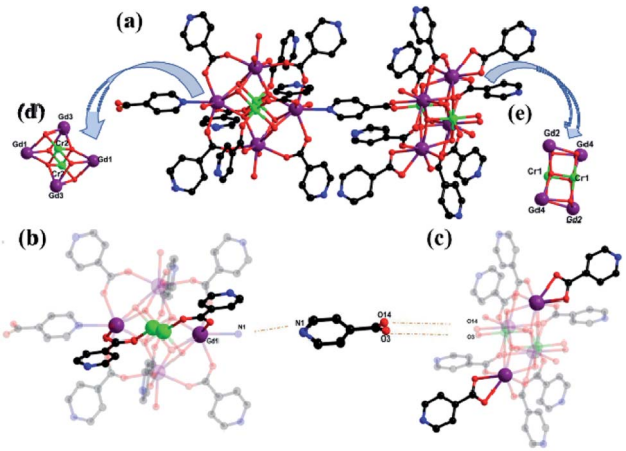

Fig. 1 The unit of **{Gd_8Cr_4}** (a), **FBU** (b) and **SBU** (c); (d) and (e) the building unit of "drum-like" **{Gd_4Cr_2}** metallic framework from different directions. For clarity, free water molecules and H atoms are omitted. Colour codes: Gd^{3+}, purple; Cr^{3+}, green; O, red; N, blue.

structure, the IN^- ligands adopt four coordination modes (**I–IV**, Fig. 2a): $\mu_3\text{-}\eta^1\text{:}\ \eta^1\text{:}\ \eta^1$; $\mu_2\text{-}\eta^1\text{:}\ \eta^1\text{:}\ \eta^0$; $\mu_2\text{-}\eta^1\text{:}\ \eta^1\text{:}\ \eta^0$; $\mu_1\text{-}\eta^1\text{:}\ \eta^0\text{:}\ \eta^0$. For mode **I**, the IN^- anion bridges one Gd^{3+} and Cr^{3+} ion and uses the nitrogen atom to bridge another Gd^{3+} ion while the IN^- anion links to one Gd^{3+} and one Cr^{3+} ion in mode **II**. For mode **III** and **IV**, the IN^- anion bridges two Gd^{3+} ions and one Gd^{3+} ion, respectively. In **FBU**, the IN^- ligands adopt four mode **II** and four mode **III**, while in **SBU**, the IN^- ligands addition to adopt two mode **II** and four mode **III**, but also in two mode **IV**, where the IN^- anions bridge one Gd^{3+} ion. Here, the ligand HIN in mode **I** functions solely as a bridging ligand, N1 on HIN is linked to Gd1 in **FBU** and carboxyl oxygen O3 and O14 are linked to Cr1 and Gd2 in **SBU**, which makes neighboring drum-like **FBU** and **SBU** connect to form unit **{Gd_8Cr_4}**. The neighboring **{Gd_8Cr_4}** units are linked by HIN forming a rare one-dimensional (1D) wave chain structure (Fig. 2b), in which the adjacent chains interact with each other by π–π stacking interactions to form a two-

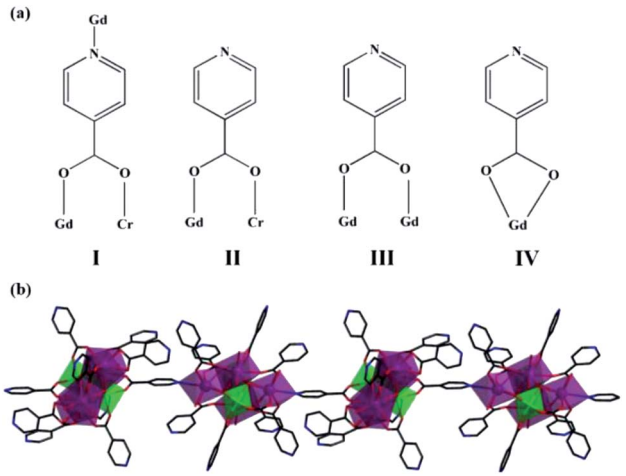

Fig. 2 (a) Four kinds of coordinate modes of HIN in **1**; (b) 1D chain structure in **1**.

dimensional (2D) layered structure between pyridyl rings and further interact with each other to build up a three-dimensional (3D) network by π–π interactions, as shown in Fig. 3.

Of the eight Gd^{3+} ions, with four coordination environments, which are all eight-coordinated (Fig. 4a–d). Among them, Gd1 is connected with seven O atoms (O11, O12, O13, N1, O6, O7, O10, O3W) from HIN ligands, bridging oxygen, and one water molecule. Gd2 is completed by three O atoms (O14, O15, O16) from HIN ligands, two water molecules (O4W, O5W) and three bridging oxygen (O1, O2, O4). Similarly, Gd3 is connected to two water oxygen (O1W, O2W), three bridged oxygen (O6, O7, O10) and three oxygen (O17, O18, O19) from HIN ligands. While Gd4 is connected to three bridged oxygen (O1, O2, O4) and the rest oxygen from HIN ligands. Beyond that, Cr^{3+} ions (Fig. 4e and f) are all six-coordinated with six oxygen atoms, and two of which are from HIN ligands and the rest are bridged oxygen. For compound **1**, the interval value of Cr–O distances are 1.974(4) to 2.057(5) Å and the Gd–O are 2.367(5) to 2.577(5) Å, which are all in line with the literatures (Table S1†).[27,32] Further, the bond angles around O–Cr–O and O–Gd–O, respectively, varying from 83.34(18) to 179.30(17)° and 51.43(17) to 148.96(14)° (Table S2†).[33]

In comparison with the previously reported hexanuclear $\{Ln_4Cr_2\}$ clusters by Zhai *et al.* in 2018,[31a] which has the same metal skeleton $\{Ln_4Cr_2\}$ as the compound we obtained. However, the reported $\{Ln_4Cr_2\}$ cluster is composed of two symmetry-related units $\{Ln_2Cr\}$, then is further linked together by sulfate ions, resulting in a 3D framework. While in this work, the two adjacent "drum-like" $\{Ln_4Cr_2\}$ cluster is related to each other by IN^- ligands, and then the carboxyl group on the ligand is bonded to the nitrogen to form a 1D chain structure, which is rare.

IR spectra

The IR spectra of the two compounds have similar infrared spectrum curves, which are presented in Fig. S5 and S6.† Taking compound **1** as an example: the strong peak at 3412 cm^{-1} could be considered as the stretching vibration of –OH. Contemporary, the sharp peak at 1608 cm^{-1} infers the existence of pyridine ring,

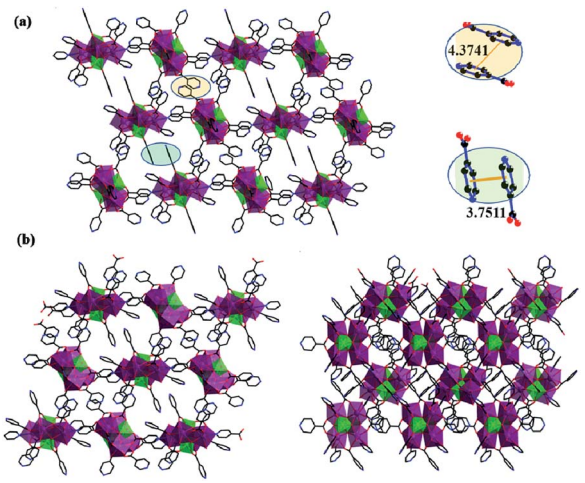

Fig. 3 (a) Two-dimensional structure of **1**; (b) three-dimensional structure of **1** (viewing from *a* axis and *c* axis).

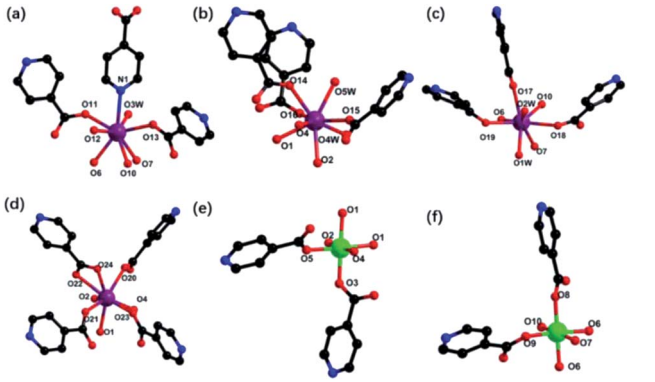

Fig. 4 (a) Ball-and-stick of coordination mode of Gd1 (a), Gd2 (b), Gd3 (c), Gd4 (d), Cr1 (e), Cr2 (f).

while the peaks at 1547 cm^{-1} and 1417 cm^{-1} are largely thanks to the anti-symmetric stretching vibration and the symmetric stretching vibration of the carboxyl group, respectively. Other peaks of compound **1**, such as peak at 774, 679, 563 cm^{-1}, showing the stretching vibration of the metal oxygen bond.

Powder X-ray diffraction

As shown in the Fig. S7 and S8,† the measured values are basically consistent with the theoretical spectrum, indicating the two compounds are pure. At the same time, slight difference in intensity can be attributed to the limitations of instrument performance or the selective orientation effect of the sample.

Thermogravimetric analysis

As shown in Fig. S9 and S10,† weight loss curves of the two compounds are semblable, which can be divided into three stages. Taking compound **2** as an example: the first mass loss of 8.52% in the temperature range of 25–140 °C is caused by the removal of free water molecules and coordination water (theoretical 8.58%); the second part of the curve remains basically unchanged between 140 and 425 °C, which maybe due to the stability of the structure; when the temperature rises above 425 °C, the entire compound skeleton gradually collapses as the organic ligand isonicotinic acid is lost.

Magnetic studies

The solid-state magnetic susceptibility ($\chi_M T - T$) of **1** was investigated between 300 and 1.8 K in an applied field of 1.0 kOe. As shown in Fig. 5, the observed $\chi_M T$ value for compound **1** at 300 K is 66.11 cm^3 K mol^{-1}, which is lower than the expected value of 70.5 calculated for eight isolated Gd^{3+} ions ($S = 7/2$, $g = 2$) and four isolated Cr^{3+} ions ($S = 3/2$, $g = 2$). With temperature dropping, the $\chi_M T$ value falling to 57.40 cm^3 K mol^{-1} at 25 K. And on further cooling, the value declines abruptly at 1.8 K and reaches a minimum of 13.14 cm^3 K mol^{-1}, which are characteristic of antiferromagnetic coupling interactions. Fitting data with the Curie–Weiss law gives parameters $C = 66.91$ cm^3 K mol^{-1} and $\theta = -4.34$ K, further confirming the antiferromagnetic coupling performance.

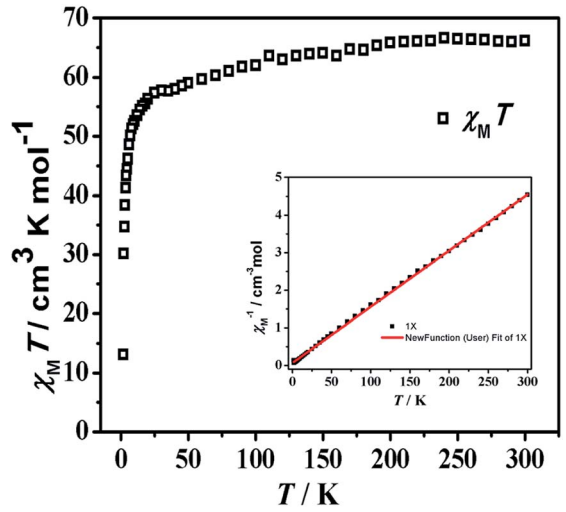

Fig. 5 Plot of $\chi_M T$ *vs.* T for **1**. Insert: Temperature dependence of $1/\chi_M$.

Magnetization measurements (M *vs.* H) of compound **1** was examined in multifarious temperatures between 1.8 and 10 K (Fig. S11†). It exhibits a rapid increase at lower filed and incline to keep jarless at 7 T. For compound **1**, the magnetization reaches 52.06 Nβ at 1.8 K and 7 T. In order to estimate the magnetocaloric effect, the Maxwell equation $\Delta S_m(T) = \int[\partial M(T, H)/\partial T]_H dH$ can be applied to calculate ΔS_m to the experimental value.[34] In Fig. 6, the magnetic entropy value has reached a value of about 14 J kg^{-1} K^{-1} at $\Delta H = 3$ T. At last, the observed maximum $-\Delta S_m$ for compound **1** of 23.40 J kg^{-1} K^{-1} is obtained at 3.0 K for $\Delta H = 7$ T, which is less than the theoretical maximum entropy value is 44.39 (based on eight isolated Gd^{3+} ions and four isolated Cr^{3+} ions calculation), owing to the feeble antiferromagnetic interactions within the metal ions.

Luminescence properties

The solid-state fluorescence spectrum of **2** was measured under different excitation wavelengths. As can be seen in Fig. 7, the Tb^{3+} compound exhibits typical photoluminescence signals. When excited at 367 nm, the solid-state fluorescence peaks for compound **2** exhibits four bands from 490 to 624 nm, which are derived from the electronic transition of Tb^{3+} between $^5D_0 \rightarrow {}^7F_j$ (j = 6, 5, 4, 3).[17,35,36] Among them, the transition of the electric dipolar of $^5D_0 \rightarrow {}^7F_6$ at 490 nm and the transition of the magnetic dipolar of the peak $^5D_0 \rightarrow {}^7F_5$ at 546 nm. Additionally, the peaks at 586 nm and 624 nm pertain to the transition of $^5D_0 \rightarrow {}^7F_4$ and $^5D_0 \rightarrow {}^7F_3$ electrons, which are agreement with literatures.[37–39]

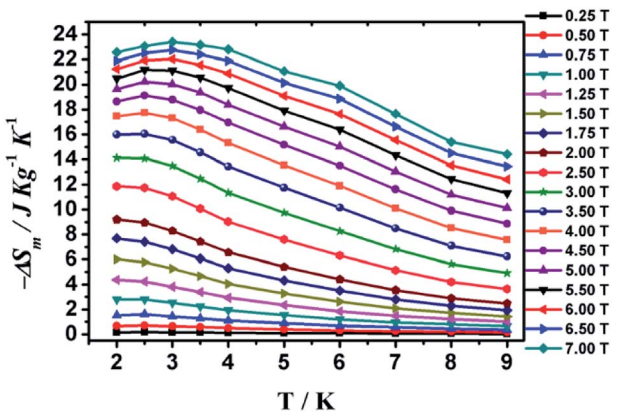

Fig. 6 Values of $-\Delta S_m$ calculated from the magnetization data for **1** at different fields and temperatures.

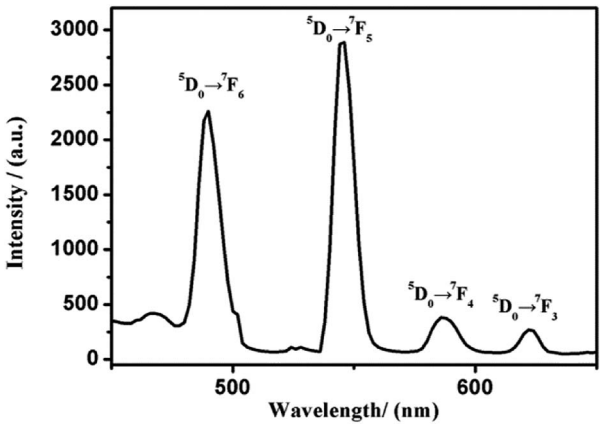

Fig. 7 The solid-state fluorescence spectrum of **2** at room temperature.

Conclusions

In brief, two twelve-nuclear compounds **{Ln_8Cr_4}** were successfully obtained by hydro-/solvothermal method, displaying one-dimensional wave chain structure, which is rare been reported before. The MCE of compound **1** is 23.40 J kg^{-1} K^{-1} at about 3.0 K and $\Delta H = 7$ T. In the meantime, fluorescence measurements of compound **2** reveal typical of Tb-based luminescence, which indicates it may be photoluminescence materials with great promise. These results enrich the existing field of Cr–Ln compounds, which played a certain driving force for the design and synthesis of molecular refrigerants.

Conflicts of interest

There are no conflicts to declare.

Acknowledgements

This work was supported by the Natural Science Foundation of Jiangsu Province (BK20191359) and China (Grant 21571103), the Major Natural Science Projects of the Jiangsu Higher Education Institution (Grant 16KJA150005).

Notes and references

1 X. Y. Zheng, Y. H. Jiang, G. L. Zhuang, D. P. Liu, H. G. Liao, X. J. Kong, L. S. Long and L. S. Zheng, *J. Am. Chem. Soc.*, 2017, **139**, 18178–181811.

2 Q. F. Lin, J. Li, Y. Y. Dong, G. P. Zhou, Y. Song and Y. Xu, *Dalton Trans.*, 2017, **46**, 9745–9749.
3 J. Dong, P. Cui, P. H. Shi, P. Cheng and B. Zhao, *J. Am. Chem. Soc.*, 2015, **137**, 15988–15991.
4 J. B. Peng, X. J. Kong, Q. C. Zhang, M. Orendač, J. Prokleška, Y. P. Ren, L. S. Long, Z. P. Zheng and L. S. Zheng, *J. Am. Chem. Soc.*, 2014, **136**, 17938–17941.
5 (*a*) X. Y. Zheng, X. J. Kong, Z. P. Zheng, L. S. Long and L. S. Zheng, *Acc. Chem. Res.*, 2018, **51**, 517–525; (*b*) X. Y. Zheng, J. Xie, X. J. Kong, L. S. Long and L. S. Zheng, *Coord. Chem. Rev.*, 2019, **378**, 222–2363.
6 C. H. Cui, J. P. Cao, X. M. Luo, Q. F. Lin and Y. Xu, *Chem.–Eur. J.*, 2018, **24**, 15295–15302.
7 X. Meng, W. Shi and P. Cheng, *Coord. Chem. Rev.*, 2019, **378**, 134–150.
8 J. Long, J. Rouquette, J. M. Thibaud, R. A. Ferreira, L. D. Carlos, B. Donnadieu, V. Vieru, L. F. Chibotaru, L. Konczewicz, J. Haines, Y. Guari and J. Larionova, *Angew. Chem., Int. Ed.*, 2015, **54**, 2236–2240.
9 M. Evangelisti and E. K. Brechin, *Dalton Trans.*, 2010, **39**, 4672–4676.
10 F. B. Yu, Q. Gao, B. Zhang, Z. X. Meng and Z. Chen, *Int. J. Refrig.*, 2003, **26**, 622–636.
11 Z. G. Gu, C. Zhan, J. Zhang and X. H. Bu, *Chem. Soc. Rev.*, 2016, **45**, 3122–3144.
12 H. L. Qian, C. X. Yang and X. P. Yan, *Nat. Commun.*, 2016, **7**, 12104.
13 Z. Y. Li, Y. L. Xu, X. F. Zhang, B. Zhai, F. L. Zhang, J. J. Zhang, C. Zhang, S. Z. Li and G. X. Cao, *Dalton Trans.*, 2017, **46**, 16485–16492.
14 R. Sibille, T. Mazet, B. Malaman and M. Francois, *Chem.–Eur. J.*, 2012, **18**, 12970–12973.
15 L. Qin, J. Singleton, W. P. Chen, H. Nojiri, L. Engelhardt, R. E. Winpenny and Y. Z. Zheng, *Angew. Chem., Int. Ed.*, 2017, **56**, 16571–16574.
16 J. W. Sharples, Y. Z. Zheng, F. Tuna, E. J. L. McInnes and D. Collison, *Chem. Commun.*, 2011, **47**, 7650–7652.
17 C. H. Cui, W. W. Ju, X. M. Luo, Q. F. Lin, J. P. Cao and Y. Xu, *Inorg. Chem.*, 2018, **57**, 8608–8614.
18 J. A. Sheikh and A. Clearfield, *Inorg. Chem.*, 2017, **56**, 2843–2848.
19 S. Biswas, A. K. Mondal and S. Konar, *Inorg. Chem.*, 2016, **55**, 2085–2090.
20 J. L. Liu, Y. C. Chen, F. S. Guo and M. L. Tong, *Coord. Chem. Rev.*, 2014, **281**, 26–49.
21 W. P. Chen, P. Q. Liao, Y. Z. Yu, Z. P. Zheng, X. M. Chen and Y. Z. Zheng, *Angew. Chem., Int. Ed.*, 2016, **55**, 9375–9379.
22 S. J. Liu, C. Cao, S. L. Yao, T. F. Zheng, Z. X. Wang, C. Liu, J. S. Liao, J. L. Chen, Y. W. Li and H. R. Wen, *Dalton Trans.*, 2017, **46**, 64–70.
23 X. Y. Zheng, J. Xie, X. J. Kong, L. S. Long and L. S. Zheng, *Coord. Chem. Rev.*, 2019, **378**, 222–236.
24 X. Y. Zheng, X. J. Kong, Z. Zheng, L. S. Long and L. S. Zheng, *Acc. Chem. Res.*, 2018, **51**, 517–525.
25 F. Torres, J. M. Hernandez and X. Bohigas, *Appl. Phys. Lett.*, 2000, **77**, 3248–3250.
26 W. P. Chen, J. Singleton, L. Qin, A. Camón, L. Engelhardt, F. Luis, R. E. P. Winpenny and Y. Z. Zheng, *Nat. Commun.*, 2018, **9**, 1–6.
27 O. Blacque, A. Amjad, A. Caneschi, L. Sorace and P. E. Car, *New J. Chem.*, 2016, **40**, 3571–3577.
28 A. McRobbie, A. R. Sarwar, S. Yeninas, H. Nowell, M. L. Baker, D. Allan, M. Luban, C. A. Muryn, R. G. Pritchard, R. Prozorov, G. A. Timco, F. Tuna, G. F. S. Whitehead and R. E. P. Winpenny, *Chem. Commun.*, 2011, **47**, 6251–6253.
29 K. S. Pedersen, G. Lorusso, J. J. Morales, T. Weyhermüller, S. Piligkos, S. K. Singh, D. Larsen, M. Schau-Magnussen, G. Rajaraman, M. Evangelisti and J. Bendix, *Angew. Chem., Int. Ed.*, 2014, **53**, 2394–2397.
30 (*a*) J. D. Leng, A. K. Kostopoulos, L. H. Isherwood, A. Ariciu, F. Tuna, I. J. Vitórica-Yrezábal, R. G. Pritchard, G. F. S. Whitehead, G. A. Timco, D. P. Mills and R. E. P. Winpenny, *Dalton Trans.*, 2018, **47**, 6361–6369; (*b*) J. Rinck, G. Novitchi, W. V. D. Heuvel, L. Ungur, Y. Lan, W. Wernsdorfer, C. E. Ason, L. F. Chibotaru and A. K. Powell, *Angew. Chem., Int. Ed.*, 2010, **49**, 7583–7587.
31 (*a*) Z. Y. Li, J. J. Zhang, S. Q. Liu, H. Zhang, Y. J. Sun, X. Y. Liu and B. Zhai, *Cryst. Growth Des.*, 2018, **18**, 7335–7342; (*b*) H. Xiang, W. G. Lu, W. X. Zhang and L. Jiang, *Dalton Trans.*, 2013, **42**, 867–870; (*c*) H. Xiang, W. G. Lu, L. Jiang, W. X. Zhang and Y. H. Lan, *Eur. J. Inorg. Chem.*, 2016, 907–912.
32 J. J. Yin, C. Chen, G. L. Zhuang, J. Zheng, X. Y. Zheng and X. J. Kong, *Inorg. Chem.*, 2020, **59**(3), 1959–1966.
33 X. F. Tan, J. Zhou, H. H. Zou, L. S. Fu and Q. L. Tang, *Inorg. Chem.*, 2017, **56**, 10361–10369.
34 T. Q. Song, J. Dong, A. F. Yang, X. J. Che, H. L. Gao, J. Z. Cui and B. Zhao, *Inorg. Chem.*, 2018, **57**, 3144–3150.
35 J. Rinck, Y. Lan, C. E. Anson and A. K. Powell, *Inorg. Chem.*, 2015, **54**, 3107–3117.
36 X. X. He, Y. Liu, Y. Lv, Y. Y. Dong, G. H. Hu, S. Zhou and Y. Xu, *Inorg. Chem.*, 2016, **55**, 2048–2054.
37 Y. M. Zhou, H. G. Zhu, Z. X. Chen, M. Q. Chen, Y. Xu, H. Y. Zhang and D. Y. Zhao, *Angew. Chem., Int. Ed.*, 2001, **40**, 2166–2168.
38 K. H. Zangana, E. M. Pineda, J. Schnack and R. E. P. Winpenny, *Dalton Trans.*, 2013, **42**, 14045–14048.
39 L. Qin, J. Singleton, W. P. Chen, H. Nojiri, L. Engelhardt, R. E. P. Winpenny and Y. Z. Zheng, *Angew. Chem.*, 2017, **129**, 16798–16801.

